The link between gas diffusion and carbonation in hardened cement pastes

V. Dutzer, W. Dridi, Stéphane Poyet, P. Le Bescop, X. Bourbon

The link between gas diffusion and carbonation in hardened cement pastes

Vincent DUTZER[1], Wissem DRIDI[1], Stéphane POYET[1], Patrick LE BESCOP[1], Xavier BOURBON[2]

[1] Den-Service d'Etude du Comportement des Radionucléides (SECR), CEA, Université de Paris-Saclay, F-91191, France

[2] Andra, Parc de la Croix Blanche, 1-7 rue Jean-Monnet, F-92298 Châtenay-Malabry cedex, France

Corresponding author: Stéphane Poyet

Address: CEA Paris-Saclay, DEN/DANS/DPC/SECR/LECBA, B158 PC25, F-91191 Gif-sur-Yvette cedex, France.

E-mail: stephane.poyet@cea.fr

Abstract

The influence of atmospheric carbonation on gas diffusion was investigated using four hardened cement pastes (CEM I, CEM III/A, CEM V/A, and a low-alkalinity binder) with common water-to-binder ratio (0.4). The diffusivity of the non-carbonated and carbonated pastes with respect to helium and nitrogen was measured at different relative humidities. Carbonation decreased the diffusivity of the CEM I paste, whereas that of the other binders significantly increased after carbonation. These results show the competition between porosity clogging and cracking induced by carbonation. The consequences of carbonation are therefore believed to depend on the considered binder. Clogging dominates in ordinary Portland cement (OPC), leading to a decrease in its transport properties after carbonation; cracking dominates in blended cements, leading to a significant increase in its transport properties after carbonation.

Keywords: Cement paste (D) - Diffusion (C) - Carbonation (C) - Blended cements (D)

1. Introduction

Atmospheric carbonation refers to the reaction between carbon dioxide (CO_2) from the atmosphere and the calcium-bearing hydrates of concretes. From a practical point of view, CO_2 diffuses into concrete, dissolves in the poral solution and then reacts with calcium ions from the poral solution to precipitate calcium carbonate ($CaCO_3$) [1,2]. The depletion of calcium in the poral solution induces the dissolution of calcium-bearing phases (including portlandite) to reach a solid-solution equilibrium. The major consequence of carbonation is the lower pH of the poral solution that creates the conditions for active corrosion of steel reinforcement [3,4]. Moreover, carbonation generates the presence of a carbonated area at the interface between the structure and the environment, the properties of which differ from the bulk. In order to assess the durability of reinforced concrete structures, it is important to understand these properties because they affect the ingress rate of aggressive species such as water, CO_2 for carbonation, or oxygen for steel-carbonation-induced corrosion.

It is generally admitted that the precipitation of calcium carbonate leads to porosity clogging and then to a decrease in transport properties. This is supported by experiments that showed the reduction in permeability and/or diffusivity during or after carbonation [5–11]. This holds true for ordinary Portland cement (OPC) despite the results of the study by Ngala & Page [12].

Unfortunately, other studies dealing with blended cements showed that carbonation can have an adverse effect on transport [13–16] *i.e.* induce a significant increase in permeability and/or diffusivity that was believed to be controlled by coarsening the pore structure [12,16–18]. Recently, Auroy *et al.* [19] measured the unsaturated water permeability of non-carbonated and carbonated hardened cement pastes and the results clearly confirmed the influence of the cement type: for OPC, permeability decreased after carbonation whereas it significantly increased for blended cements. This result could be not explained by the coarsened pore structure, but rather by a competition between porosity clogging (leading to a decrease in permeability) and microcracking induced by carbonation [14,20–22].

This article presents the results of a companion study to the study by Auroy *et al*. [19] in which we have focused on the effect of carbonation on gas diffusion. The gas diffusivity of four hardened cement pastes was measured using non-carbonated and carbonated specimens. Four different binders (three of them including supplementary cementing materials) were selected to highlight their influence on carbonation and diffusivity. The results confirmed the competition between cracking and porosity clogging and the influence of the cement type. Lastly, the results were used as input data in Papadakis' model [23,24] to assess the influence of diffusivity on the carbonation rate of the pastes. Some of the results of this article were already published and are then only briefly presented hereafter. Whenever needed, the reader is referred to Auroy et al. [19] for more detail.

2. Methods

2.1. Materials

The four hardened cement pastes prepared and tested by Auroy *et al*. [19] were used in this study. They consisted in pastes prepared with OPC, CEM III/A (mix of OPC and slag); CEM V/A (mix of OPC, slag and fly ash) and a low-alkalinity cement (LAC, made with OPC, fly ash and silica fume, see Table 1). The water-to-binder ratio was fixed at 0.40 for all the pastes because it provided good fluidity and stability of the fresh mix.

Table 1: composition of the cement pastes (wt%)

Compound	CEM I	CEM III/A	CEM V/A	LAC
CEM I	100%	39%	56%	37.5%
Slag	-	61%	22%	-
Fly ash	-	-	22%	30%
Silica fume	-	-	-	32.5%
Superplasticizer Chryso®Fluid Optima 175	-	-	-	1% of binder
Water-to-binder ratio	0.40	0.40	0.40	0.40

The pastes were prepared in 2 L batches (in three consecutive batches) and cylindrical specimens were cast (Ø50 × 100 mm) that were unmoulded two weeks after casting. They were then kept for four more months in closed containers, immersed in a specific solution with a composition designed to prevent leaching (see [25] and [19] for more detail). Finally, the cylinders were cut into 6 mm-thick disks that were tested for water permeability [19] and gas diffusion (in this study).

2.2. Accelerated carbonation

Carbonation was achieved using a specific device that was first designed and set up for another study [26,27]. This device comprises a commercial environmental chamber for temperature and relative humidity (RH) control, and an automated system for CO_2 measurement and control.

Prior to carbonation, all the disks were left one month in a climatic chamber at 25°C and 55% RH not to reach but to get close to hygral equilibrium. In the first days, the RH in the chamber was decreased in small steps (5%) from 95% RH to 55% RH to prevent the disks from cracking due to drying shrinkage. All the disks were assumed to be unaffected by carbonation at the end of this phase but this was not verified anyhow. The disks were then placed in the accelerated carbonation chamber and carbonated at 25°C ± 0.2°C, 55% RH ± 1% and 3.0% CO_2 ± 0.2%. These conditions were selected to accelerate carbonation while being representative of natural carbonation [28–30]. The disks were left for one year in the chamber, and thermogravimetric analysis (TGA) was used to verify that they were fully carbonated afterwards [19].

2.3. Gas diffusion test

The diffusivity of helium and nitrogen was measured using the through-diffusion method [31,32]. This involved putting the cement paste disk between two compartments filled with two different gases, previously generated at a fixed/common RH. The upstream chamber was filled with helium (100% He) and the downstream with pure nitrogen (100% N_2), both at atmospheric pressure (Figure 1). For each sample, the test was conducted at a different RH (Table 2) in order to characterize the dependency of gas diffusivity with RH. It must be noted that due to the presence of water vapour in the upstream and downstream chambers, the initial gas concentrations (He and N_2) lied between 97.7% and 99.9% depending on the considered RH value.

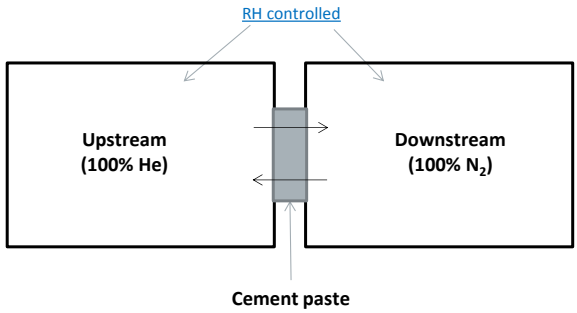

Figure 1: principle of the gas diffusion test

For the purpose of this test, 6 mm-thick discs (Ø50 mm) were first resaturated under water and vacuum and then and equilibrated at different RH values and ambient temperature using saturated salt solutions (see section 2.4). At equilibrium, each specimen was sealed into position using an epoxy adhesive and O-rings to avoid leakage. During the test, helium and nitrogen counters were diffused through the sample and the gas composition in the two compartments was frequently monitored by gas chromatography analysis. The results were analysed on the basis of Fick's second law in 1D (j = He or N_2):

$$\frac{\partial P_{gj}}{\partial t} = \frac{D_e^j}{\phi(1-S)}\left(\frac{\partial^2 P_{gj}}{\partial x^2}\right) \quad (1)$$

where P_{gj} and D_e^j are the partial pressure and effective diffusion coefficient of the gas j; ϕ and S are the material porosity and saturation degree. Liquid diffusion was neglected in this equation. The experimental results for each gas were fitted using the analytical solution of the diffusion equation [33], making use of regression analysis to determine the effective diffusion coefficient.

2.4. Water retention curves, mineralogy, microstructure & cracking

The water retention curves were acquired using the desiccator method [34,35]: disks were resaturated under water and vacuum and then placed in different desiccators above saturated salt solutions. At equilibrium (when the disk mass was constant or almost), the saturation S was computed using:

$$S(h) = \left(\frac{\Delta m}{m}\right)(h) + \frac{\emptyset}{d_{sat}} \quad (2)$$

where $\left(\frac{\Delta m}{m}\right)(h)$ is the relative mass variation of the disks at equilibrium with the relative humidity h; ϕ the porosity and d_{sat} the saturated density of the paste.

Table 2: saturated salt solutions and resulting RH at 20°C [36–39]

Saturated salt solution	Formula	RH at 20°C
Calcium chloride	$CaCl_2$	≈ 3%
Lithium chloride	LiCl	11%
Potassium acetate	$C_2H_3KO_2$	23%
Magnesium chloride	$MgCl_2$	33%
Potassium carbonate	K_2CO_3	43%
Magnesium nitrate	$Mg(NO_3)_2$	54%
Sodium bromide	NaBr	59%
Ammonium nitrate	NH_4NO_3	63%
Potassium iodide	KI	70%
Ammonium chloride	NH_4Cl	80%
Potassium nitrate	KNO_3	92%
Potassium sulfate	K_2SO_4	98%
Deionized water	H_2O	100%

The C-S-H concentration was assessed using the method proposed by Olson & Jennings [40] that relates the water content at 20% RH and the C-S-H amount. However, we did not strictly follow the experimental protocol that we found too complicated (too many different operations) and time-consuming. Rather, we took advantage of the desorption isotherms that were acquired (Figure 3) to estimate the water content at 20% RH using the model proposed by Pickett [41]:

$$w(h) = \frac{Cw_m}{(1-h)} \frac{(1-h^n)h + bnh^n(1-h)}{(1-h)+C(h+bh^n)} \quad (3)$$

where

- C is a positive parameter related to the energy of adsorption of the first water layer
- w_m water content needed to complete the monolayer
- n maximal number of layers
- b constant related to the rate of condensation/evaporation
- h relative humidity
- w water content of the paste (wt%)

Because the amount of water retained is higher in desorption than in adsorption [34], using the desorption isotherm to estimate the water content at 20% RH was thought to have overestimated the C-S-H content.

The amount of portlandite was measured using thermogravimetric analysis [42]: 120 mg of powdered paste was heated at 10°C/min up to 1150°C under a nitrogen flow (80 mL/min). The amount of portlandite was then quantified using the stepwise method [43].

The pore size distribution was characterised using mercury intrusion porosimetry (MIP). Some paste samples were first crushed into pieces (several mm large) that were frozen with liquid nitrogen and then dried under vacuum for seven days. The mercury maximal pressure was 414 MPa so that the smallest pores investigated were 3 nm in diameter.

In order to highlight and quantify microcracking, some disks were embedded in a fluid resin that included a fluorescent dye. Pictures of the disk surfaces were taken under ultraviolet light and the images were processed to evaluate the surface fraction of the cracks using [19]:

$$I_c = \frac{\text{Number of pixels attributed to the cracks}}{\text{Total number of pixels of the disk surface}} \quad (4)$$

The carbonated pastes were tested just after carbonation whereas the non-carbonates ones were tested after being dried at 55% RH and 25°C.

3. Results

3.1. Mineralogy, microstructure

Table 3 presents the mineralogical composition of the non-carbonated pastes (in terms of portlandite & C-S-H contents). It is noteworthy that the C-S-H content increased when the portlandite content decreased because of pozzolanic reactions. This not only resulted in the refinement of the pore structure of the pastes with mineral additions compared with CEM I (Figure 2), but also in an increase in the total porosity (Table 4). The water retention curve of the blended cements subsequently exhibited a much more pronounced plateau at high RHs, together with a higher monolayer knee with regards to CEM I associated with the refined pore structure and higher specific surface area respectively.

Table 3: CH and C-S-H content of the hardened cement pastes (not carbonated).

	CEM I	CEM III/A	CEM V/A	LAC	Unit
[CH]	5.3	1.8	2.3	0.0	mol/L
[C-S-H]	2.6	3.2	3.2	3.8	mol/L

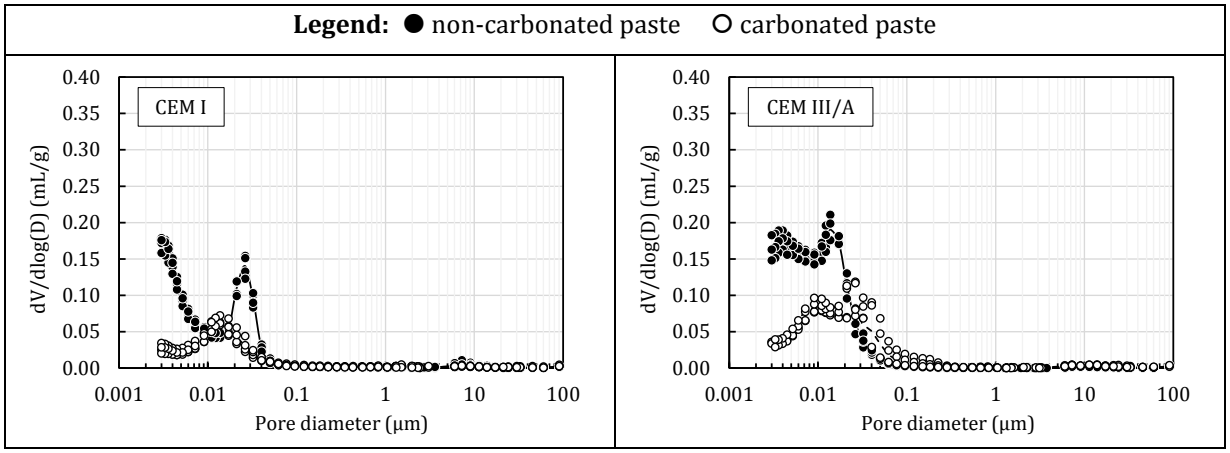

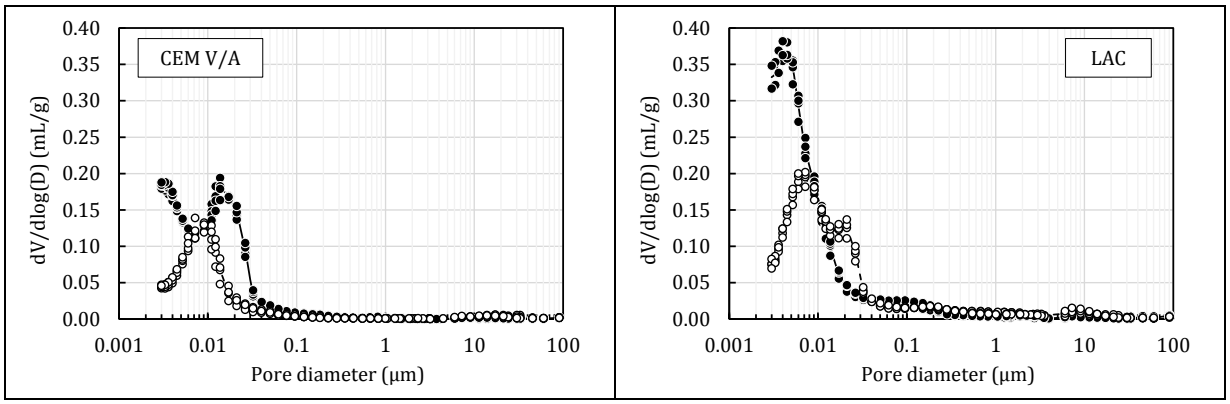

Figure 2: Pore-size distribution of the pastes (results already published in [19])

Carbonation (and consequent CO_2 fixation) led to an increase in the paste density and then to a decrease in the porosity (Table 4). Note that the porosity decrease was less pronounced in the case of the binders with mineral additions (and was lowest for the low-alkalinity cement), mainly because the amount of available calcium was reduced by the mineral additions. The pore size distribution of the pastes was modified accordingly (Figure 2): the number of pores was reduced across the entire pore range. Note that the critical pore diameter increased slightly after carbonation for the CEM III/A and LAC pastes. The water retention of the CEM I paste hardly changed after carbonation, whereas that of the blended cement pastes was strongly modified: saturation was always lower after carbonation and the plateau at high RH disappeared (Figure 3).

Table 4: porosity and density of the hardened cement pastes.

Cement paste		CEM I	CEM III/A	CEM V/A	LAC	Unit
Non-carbonated	Porosity	36.3%	39.8%	36.9%	41.0%	%
	Density (saturated)	2.05	2.00	1.93	1.77	-
Carbonated	Porosity	21.1%	29.3%	27.6%	35.5%	
	Density (saturated)	2.29	2.19	2.16	1.91	

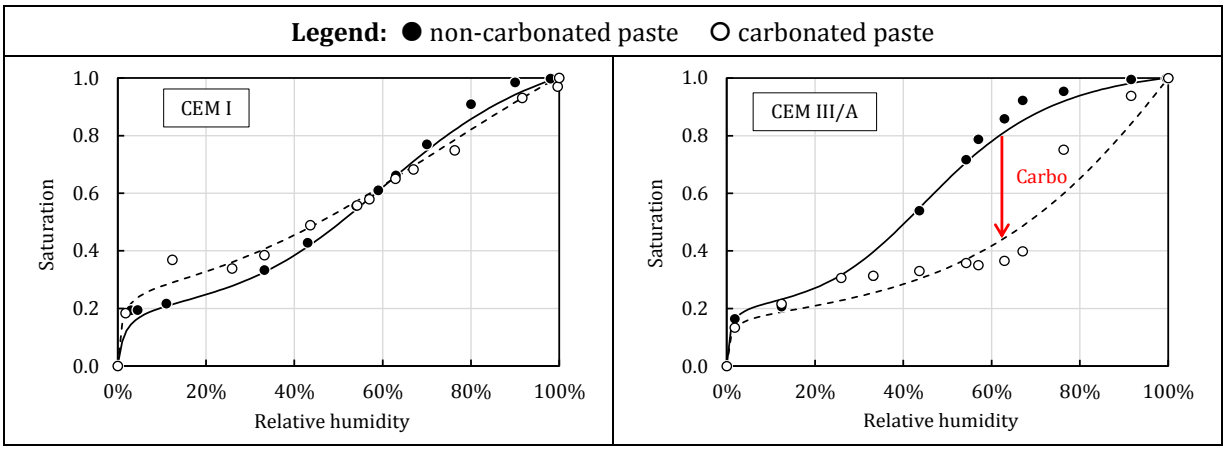

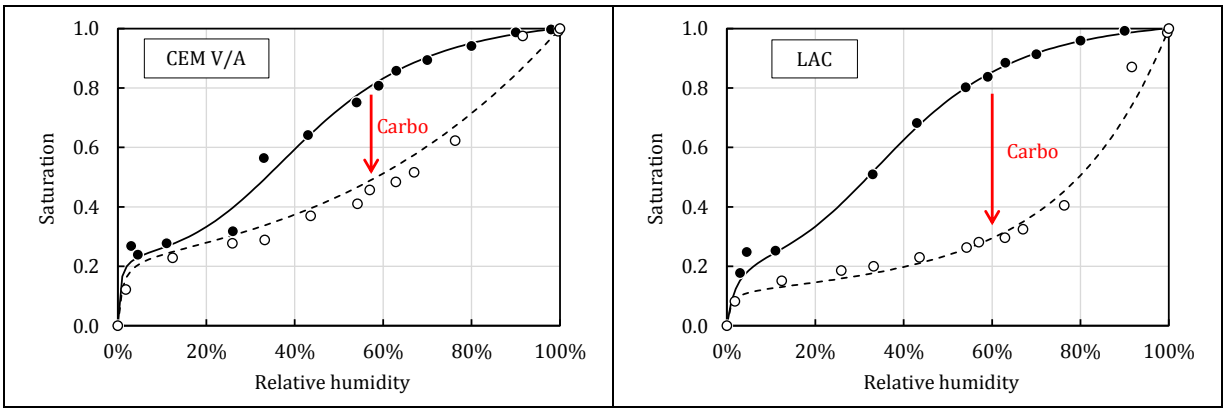

Figure 3: desorption isotherms (results already published in [19])

3.2. Cracking

Figure 4 shows the surfaces of non-carbonated and carbonated disks. The non-carbonated pastes appeared to be free of cracks (I_c = 0%) whereas the carbonated pastes revealed a network of fine cracks. An average crack opening of 10-15 µm was measured for all the pastes using optical microscopy. The cracking index I_c confirmed that the cracking intensity depended on the binder and the mineralogical assemblage (mainly CH and C-S-H).

	Non-carbonated pastes			Carbonated pastes		
	Raw image	Thresholded image	*Ic*	Raw image	Thresholded image	*Ic*
PI (CEM I)	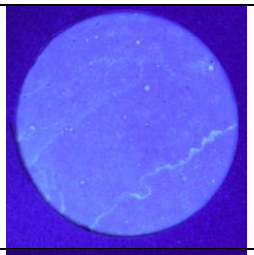	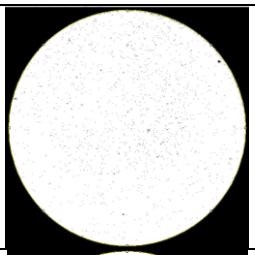	0%	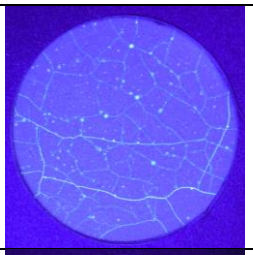	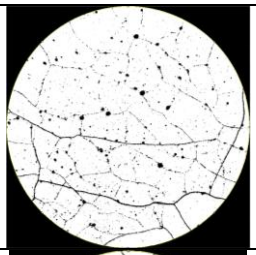	4%
PIII (CEM III/A)	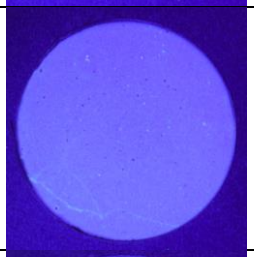	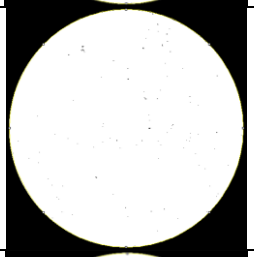	0%	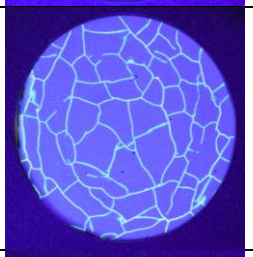	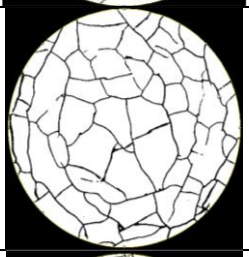	9%
PV (CEM V/A)	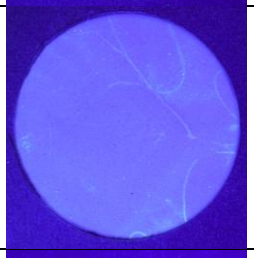		0%	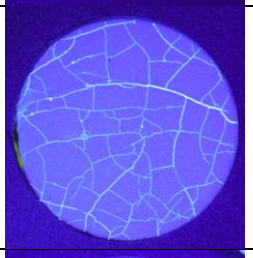	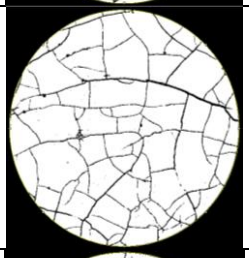	7%
LAC	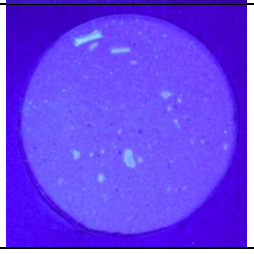	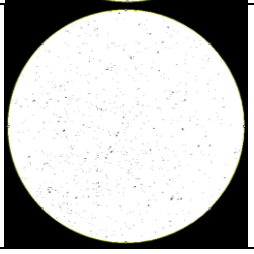	0%	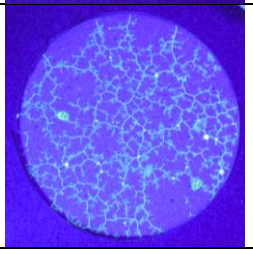	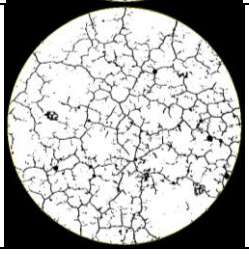	10%

Figure 4: cracking of the pastes after carbonation (results already published in [19])

3.3. Gas diffusion

Figure 5 presents helium diffusivity versus saturation for the four cement pastes (carbonated and non-carbonated). All the tested cement pastes exhibited a common behaviour. At low saturation, the gas diffusion coefficient remained constant up to a critical saturation value (between 0.5 and 0.7 depending on the considered cement and whether the paste was carbonated or not). Beyond this critical saturation value, there was a drop in the gas diffusion coefficient due to water condensation in capillary pores that slowed down gas diffusion [31,32,44][45]. The reader should nevertheless be aware that beyond the critical saturation value, the available results may not be sufficient to counterbalance the experimental scatter and therefore should be considered with caution.

The effect of carbonation on gas diffusion was not the same for all the pastes. The gas diffusivity of the CEM I pastes was reduced three fold after carbonation, whereas that of the blended cements was significantly increased (multiplied by 3, 10 and 100 for the CEM III/A, CEM V/A and LAC respectively). These results are consistent with those of Auroy *et al*. [19] for permeability and thus support their findings.

The difference in critical saturation values could be related to the modification of the desorption isotherm. The critical saturation for the CEM I paste remained unmodified by carbonation in relation to the water retention curve which also barely changed after carbonation. The critical saturation value for the blended cements shifted from 0.5-0.6 to 0.6-0.7; this was related to the change in the desorption isotherm that shifted capillary condensation at higher RH (Figure 3).

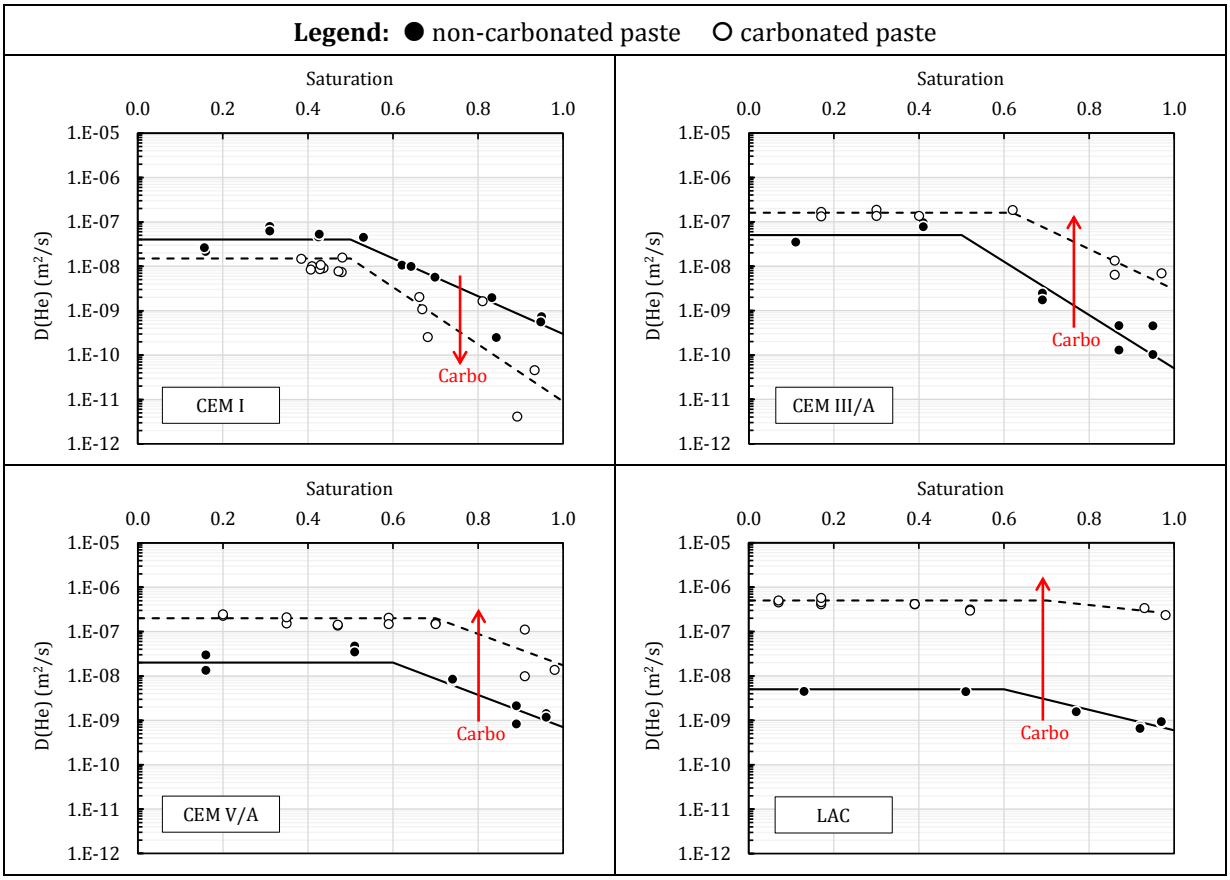

Figure 5: D(He) of the non-carbonated and carbonated

Figure 6 plots the ratio of helium diffusivity $D(\mathrm{He})$ to that of nitrogen $D(\mathrm{N_2})$ and provides valuable information on the diffusion regime during the tests. Knudsen diffusion occurs in narrow pores when the mean free path of the gas molecules is greater than the pore diameter and when the molecules collide with the pore walls. Assuming that Knudsen diffusion is indeed the means of diffusion in this case, the $D(\mathrm{He})/D(\mathrm{N_2})$ ratio only depends on the molecular mass of the gases [46,47] and is equal to 2.67:

$$\text{Knudsen diffusion } \frac{D(\mathrm{He})}{D(\mathrm{N_2})} = \sqrt{\frac{M(\mathrm{N_2})}{M(\mathrm{He})}} = 2.67 \tag{5}$$

where $M(\mathrm{N_2})$ and $M(\mathrm{He})$ are the molecular masses of $\mathrm{N_2}$ (14.01) and He (4.00) respectively.

Conversely, molecular diffusion dominates in pores larger than the mean free path. When molecular diffusion is the only motion involved, the $D(\mathrm{He})/D(\mathrm{N_2})$ ratio depends on the diffusivity of one gas through the other [46,47]:

$$\text{Molecular diffusion } \frac{D(\mathrm{He})}{D(\mathrm{N_2})} = \frac{D(\mathrm{He/N_2})}{D(\mathrm{N_2/He})} = 1.0 \tag{6}$$

where $D(\mathrm{He/N_2})$ is the diffusivity of He through $\mathrm{N_2}$ and $D(\mathrm{N_2/He})$ the diffusivity of $\mathrm{N_2}$ through He, yet by definition, the two are equal.

It was interesting to note in Figure 6 that most of the values obtained for all the non-carbonated pastes lay between 1.0 (molecular diffusion) and 2.67 (Knudsen diffusion), indicating that diffusion was dominated by neither molecular diffusion nor Knudsen diffusion, but rather involved the two of them. This was assumed to be due to the pore-size distribution of the four pastes including connected pores up to roughly 100 nm (simultaneous presence of pores smaller and larger than the gas mean free path, see Figure 2. Once carbonated, however, the diffusion through the pastes appeared to be dominated by molecular diffusion (the $D(\mathrm{He})/D(\mathrm{N_2})$ ratio became almost 1 whatever the saturation). This indicates that the gas molecules were able to diffuse through a new pathway (other than the pore network) with dimensions greater than their mean free path; this is consistent with the presence of cracks observed on the disk surfaces (Figure 4).

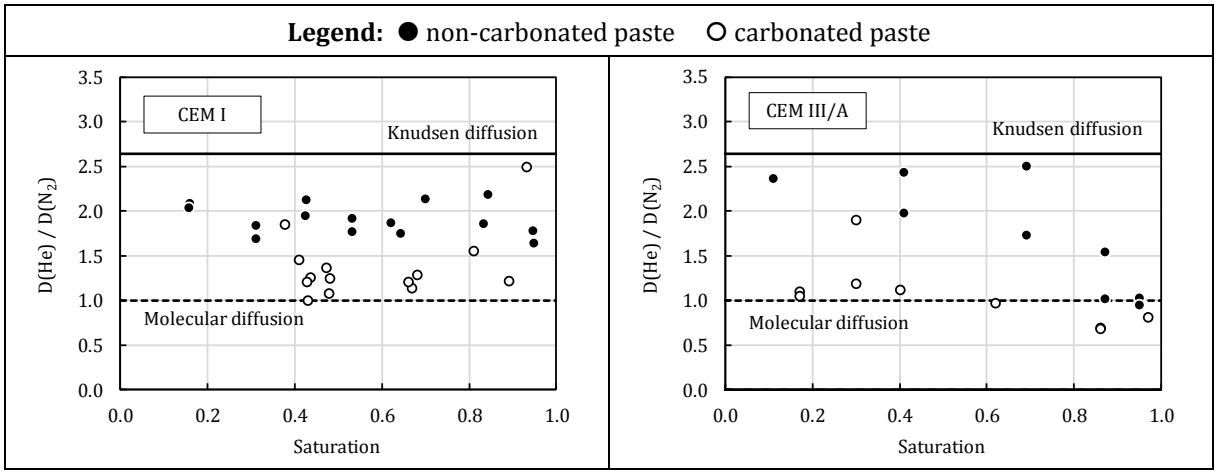

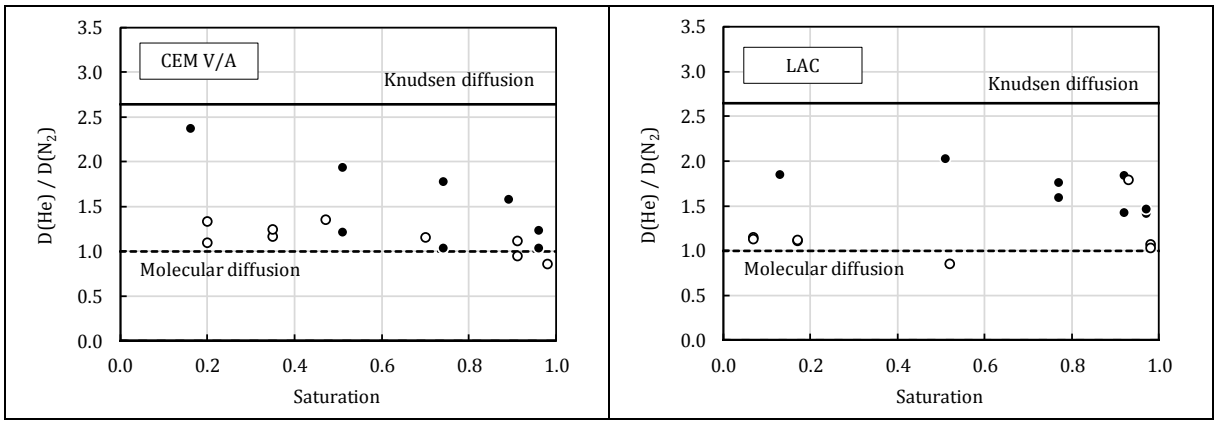

Figure 6: ratio D(He)/D(N_2)

4. Discussion

Figure 7 compares the diffusivity (*i.e.* the value obtained at the plateau) obtained for the non-carbonated pastes. It is interesting to note that the diffusivity decreased when the C-S-H content increased because of the pore refinement induced by pozzolanic reactions (Figure 2). This has been long known for slag and fly ash [31,48,49].

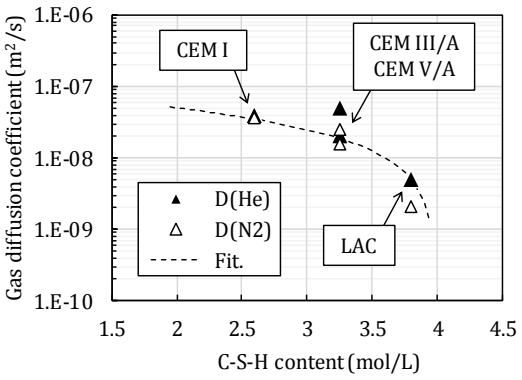

Figure 7: Comparison of gas diffusivity in the non-carbonated pastes (the broken line is only used to highlight the trend)

In order to compare the effect of carbonation on gas diffusion, the diffusivity ratios of the carbonated pastes to those of the non-carbonated were calculated and plotted in Figure 8, together with the permeability results obtained by ref. [19]. It is recalled that the value of the cracking index I_c increases with the number and surface of cracks on the specimen surface - see ref. [19] for more detail. It is interesting to note that the ratio was lower than one for OPC indicating that the transport properties of the carbonated CEM I paste were lower than those of the non-carbonated paste. In this case, porosity clogging prevailed over microcracking. The carbonated/non-carbonated ratio was greater than one for binders with SCM and it increased with the cracking index. The diffusion results more or less followed the same trend as permeability. This unambiguously points to the fact that cracking was the major cause of the increase in transport properties after carbonation for binders with SCM. This confirmed the results obtained in the previous study of Auroy *et al.* [19] but was in contradiction with others [16,18] that reported coarsening of the pore structure after carbonation.

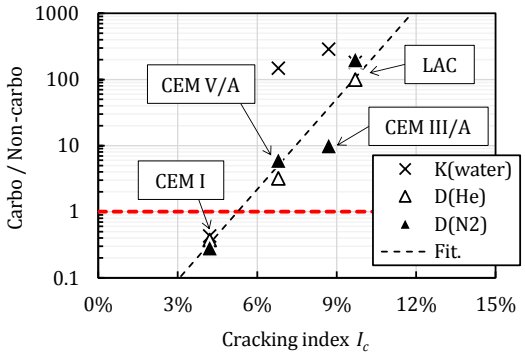

Figure 8: increase in the transport properties of the pastes after carbonation, including the permeability results of Auroy et al. [19]

Mineral additions such as fly ash, slag and silica fume are known to increase the carbonation rate [50,51]. This increase is generally attributed to the decrease in CO_2 buffer capacity (aka alkalinity reserve, *i.e.* the amount of calcium-bearing phases that can be carbonated) [52–56]. The significant cracking observed in this study was however likely to accelerate CO_2 diffusion through the carbonated zone and then increase the carbonation rate. We tried to assess the respective contribution of these two phenomena using the experimental data acquired in this study and a simple modelling approach. Our goal was not to obtain accurate estimations using the most up to date models and information, but rather, using a simplified approach that catches the main features of carbonation, to obtain rough estimates to check whether one phenomenon dominates over the other.

First assuming that diffusion is the carbonation rate-controlling process and assuming a steady-state, the progress in the carbonation depth x in a semi-infinite medium versus time is written as follows [23,50,57–60]:

$$x = k\sqrt{t} \tag{7}$$

where k is the carbonation rate (mm/y$^{0.5}$). Following the work of Papadakis *et al.* [23,24] the carbonation rate k can be written under the following simple form:

$$k = \sqrt{\frac{2D^c(CO_2)[CO_2]}{[CH]^0 + 3[C\text{-}S\text{-}H]^0}} \tag{8}$$

where $D_c(CO_2)$ is the CO_2 diffusivity in the carbonated zone (m^2/s); $[CO_2]$ the CO_2 concentration in the atmosphere (mol/m^3); $[CH]^0$ and $[C\text{-}S\text{-}H]^0$ are the portlandite and C-S-H concentrations in the non-carbonated material (mol/m^3). Here, portlandite and C-S-H are implicitly assumed to be the only two calcium-bearing phases involved in carbonation. The other phases (ettringite for example or calcium aluminates) are not accounted for. It must be recalled that the amount of Ca-bearing phases that can be carbonated depends on RH which is not accounted in Papadakis' approach. This simple model is then only valid for high RH: above 50% RH, see fig. 8 in [23]. In addition, the CO_2 diffusion coefficient is implicitly assumed to be constant within the carbonated zone. This comes into contradiction with experimental observations [61–63] that show that the kinetics of dissolution-precipitation reactions do have an influence on the carbonation rate and the transfer properties evolution in the carbonated zone [64]. Please note that, according to Papadakis *et al.* [23], the C-S-H are considered to be in the form C_3-S_2-H_3 which may be more or less well suited for the OPC and part of the blended cements [65–68] but not for the LAC [69,70].

Despite these weaknesses, Papadakis' simple approach proved to be able to evaluate correctly the carbonation rates of Portland cement and Portland cement blended with fly ash or silica fume [23,71,72]. It must also be pointed out that the C-S-H concentration was assessed using the approach proposed by Olson & Jennings [40] which is based on a slightly different C-S-H formula ($C_{3.4}$-S_2-H_3) that presents similar drawbacks. All this has introduced some uncertainty into the calculations that were not evaluated, but it was not the purpose of this paper to discuss these shortcomings.

In order to compare different cement-based materials, the ratio of the carbonation rate of the material *i* to that of CEM I can be easily calculated according to:

$$R_i = \frac{k(i)}{k(CEM\ I)} = \underbrace{\left(\sqrt{\frac{[CH]_I^0 + 3[C\text{-}S\text{-}H]_I^0}{[CH]_i^0 + 3[C\text{-}S\text{-}H]_i^0}}\right)}_{R_i^m} \underbrace{\left(\sqrt{\frac{D_i^c(CO_2)}{D_I^c(CO_2)}}\right)}_{R_i^d} = R_i^m R_i^d \tag{9}$$

Doing so, it can be seen that two distinct terms appear: the first (R_i^m) accounts for the influence of the mineralogical composition (*i.e.* the CO_2 buffer capacity or alkalinity reserve), whereas the second (R_i^d) accounts for the influence of diffusion (*i.e.* the speed at which CO_2 is transported through the carbonated area). Ratio of CO_2 diffusivities is assumed to be close to that of He. The impact of CO_2 reactivity is not considered in the effective diffusivity but in the retardation factor (apparent diffusivity). Thus, this ratio only depends on the geometric factors of the samples. The latter are supposed to be insensitive to molecular size of the diffusing species.

Figure 9 indicates the values that were obtained for the ratio R_i using the CH and C-S-H contents of Table 3 and the diffusivities D(He) (described as piecewise functions of saturation) from Figure 5. It is worth noting that, at ambient RH (*i.e.* 60%), the CEM III/A and CEM V/A pastes are expected to carbonate 4 times faster than the CEM I while the LAC pastes are expected to carbonate about 8 times faster, in the same RH and pCO_2 conditions. The values of CEM V/A and CEM III/A are consistent (similar orders of magnitude) with the results obtained by Lye *et al*. for cement pastes of the same water-to-cement ratio (0.40) including slag [73] and fly ash [74] based on a comprehensive compilation of published results (with great scatter). The average acceleration for indoor carbonation was about 2.5 for the fly ash cements (clinker content between 35% and 67%wt) and the slag cements (clinker content between 36% and 65%wt) with reference to OPC.

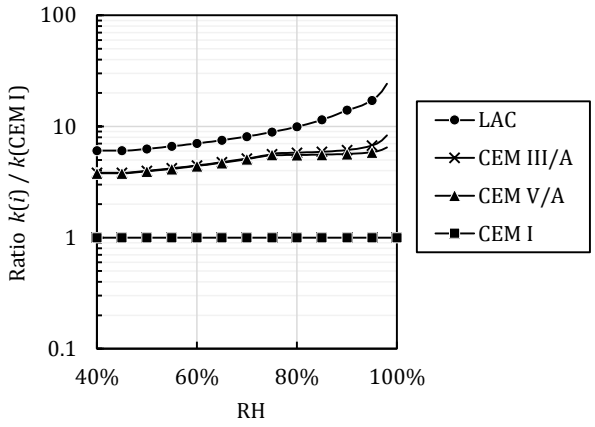

Figure 9: carbonation rate as a function of RH according to eq. (9)

Another point of interest was that this simple carbonation model allowed separating the effect of the mineralogical composition on one side and gas diffusion on the other side through the computation of the terms R_i^m and R_i^d respectively. For all the SCM bearing binders, using the data from Table 3 it was plain to see that the value of R_i^m remained very close to 1 (between 1.04 and 1.07) indicating that the change in mineralogy almost had any influence on the estimated carbonation rate. Oppositely, the values of R_i^d were much higher (around 4) which clearly indicated that the change in diffusivity was likely to be the major cause of the increase in carbonation rate when siliceous SCM are used.

Conclusion

The influence of carbonation on gas diffusion was investigated using four hardened cement pastes (CEM I, CEM III/A, CEM V/A and a low-alkalinity binder) with common water-to-binder ratio (0.4). The diffusivity to helium and nitrogen of the non-carbonated and carbonated pastes was measured at different relative humidities. Carbonation decreased the diffusivity of the CEM I paste whereas that of the other binders significantly increased after carbonation. These results are in accordance with those of Auroy *et al*. [19] (permeability) and confirm the competition between porosity clogging and cracking induced by carbonation. The consequence of carbonation are then believed to depend on the considered binder and the consequent initial mineralogical assemblage (balance between portlandite and C-S-H). For OPC, clogging dominates leading to the decrease in transport properties after carbonation whereas cracking dominates for blended cements leading to significant increase in transport properties after carbonation.

Taking profit of the experimental data acquired and using Papadakis' model [23,24], it was possible to assess the impact of the change in diffusivity on the carbonation rate of the four pastes. This made it possible to provide new elements to discuss why the carbonation rate of the blended cements is higher than that of OPC: this might be due to the significant cracking induced by carbonation that might allow allows CO_2 to diffuse through the carbonated layer faster than in OPC. The differences in initial mineralogy (CH and C-S-H) might then have a negligible impact.

These results were acquired using hardened cement pastes and it is at that point to state whether the presence of aggregates would affect the conclusions. In concretes, carbonation is expected to induce cracking of the paste embedding the aggregates but the presence of aggregates might change the spatial distribution of the cracks and mitigate the increase in transport properties. The following step is then to test concretes in the same way.

Acknowledgments

This study was part of a project funded by the French National Radioactive Waste Management Agency (Andra). Support from the French Alternative Energies and Atomic Energy Commission (CEA) is also gratefully acknowledged.

References

[1] H.F.W. Taylor, Cement chemistry, 2nd ed., Academic Press, London (UK), 1990. doi:10.1016/S0958-9465(98)00023-7.

[2] W.F. Cole, B. Kroone, Carbon dioxide in hydrated Portland cement, J. Am. Concr. Inst. 56 (1960) 1275–1296.

[3] L. Bertolini, B. Elsener, P. Pedferri, R. Polder, Corrosion of steel in concrete - prevention, diagnosis, repair, Wiley, 2004.

[4] M. Stefanoni, U. Angst, B. Elsener, Corrosion rate of carbon steel in carbonated concrete – A critical review, Cem. Concr. Res. 103 (2018) 35–48. doi:10.1016/j.cemconres.2017.10.007.

[5] M. Daimon, T. Akiba, R. Kondo, Through pore size distribution and kinetics of the carbonation reaction of Portland cement mortars. J Am Ceram Soc, J. Am. Ceram. Soc. 54 (1971) 423–428.

[6] G.R. Martin, A method for determining the relative permeability of concrete using gas, Mag. Concr. Res. 38 (1986) 90–94.

[7] P.J. Dewaele, E.J. Reardon, R. Dayal, Permeability and porosity changes associated with cement grout carbonation, Cem. Concr. Res. 21 (1991) 441–454.

[8] P.A. Claisse, H. El-Sayad, I.G. Shaaban, Permeability and pore volume of carbonated concrete, ACI Mater. J. 96 (1999) 378–381.

[9] W.P.S. Dias, Reduction of concrete sorptivity with age through carbonation, Cem. Concr. Res. 30 (2000) 1255–1261. doi:10.1016/S0008-8846(00)00311-2.

[10] H.W. Song, S.J. Kwon, Permeability characteristics of carbonated concrete considering capillary pore structure, Cem. Concr. Res. 37 (2007) 909–915. doi:10.1016/j.cemconres.2007.03.011.

[11] S.H. Jung, M.K. Lee, B.H. Oh, Measurement device and characteristics of diffusion coefficient of carbon dioxide in concrete, ACI Mater. J. 108 (2011) 589–595. doi:10.14359/51683461.

[12] V.T. Ngala, C.L. Page, Effects of carbonation on pore structure and diffusional properties of hydrated cement pastes, Cem. Concr. Res. 27 (1997) 995–1007.

[13] P. Chindaprasirt, S. Rukzon, V. Sirivivatnanon, Effect of carbon dioxide on chloride penetration and chloride ion diffusion coefficient of blended Portland cement mortar, Constr. Build. Mater. 22 (2008) 1701–1707. doi:10.1016/j.conbuildmat.2007.06.002.

[14] P.H.R. Borges, J.O. Costa, N.B. Milestone, C.J. Lynsdale, R.E. Streatfield, Carbonation of CH and C-S-H in composite cement pastes containing high amounts of BFS, Cem. Concr. Res. 40 (2010) 284–292. doi:10.1016/j.cemconres.2009.10.020.

[15] S. Zhang, B. Zhao, Research on chloride ion diffusivity of concrete subjected to CO2 environment, Comput. Concr. 10 (2012) 219–229.

[16] A. Leemann, R. Loser, B. Münch, P. Lura, Steady-state O2 and CO2 diffusion in carbonated mortars produced with blended cements, Mater. Struct. 50 (2017) 247. doi:10.1617/s11527-017-1118-3.

[17] M. Thiéry, V. Baroghel-Bouny, A. Morandeau, P. Dangla, Effect of carbonation on the microstructure and the moisture properties of cement-based materials, in: F. Skoczylas, C.A. Davy, F. Agostini (Eds.), Transf. 2012, Lille (France), 2012: pp. 1–12. doi:10.1117/1.OE.55.1.XXXXXX.

[18] A. Morandeau, M. Thiéry, P. Dangla, Impact of accelerated carbonation on OPC cement paste blended with fly ash, Cem. Concr. Res. 67 (2015) 226–236. doi:10.1016/j.cemconres.2014.10.003.

[19] M. Auroy, S. Poyet, P. Le Bescop, J.M. Torrenti, T. Charpentier, M. Moskura, X. Bourbon, Impact of carbonation on unsaturated water transport properties of cement-based materials, Cem. Concr. Res. 74 (2015) 44–58. doi:10.1016/j.cemconres.2015.04.002.

[20] J. Han, W. Sun, G. Pan, W. Caihui, Monitoring the evolution of accelerated carbonation of hardened cement pastes by X-Ray Computed Tomography, J. Mater. Civ. Eng. 25 (2013) 347–354.

[21] K. Wan, Q. Xu, Y. Wang, G. Pan, 3D spatial distribution of the calcium carbonate caused by carbonation of cement paste, Cem. Concr. Compos. 45 (2014) 255–263. doi:10.1016/j.cemconcomp.2013.10.011.

[22] M. Auroy, S. Poyet, P. Le Bescop, J.-M. Torrenti, T. Charpentier, M. Moskura, X. Bourbon, Comparison between natural and accelerated carbonation (3% CO2): impact on mineralogy, microstructure, water retention and cracking, Cem. Concr. Res. 109 (2018) 64–80. https://doi.org/10.1016/j.cemconres.2018.04.012.

[23] V.G. Papadakis, C.G. Vayenas, M.N. Fardis, Fundamental modeling and experimental investigation of concrete carbonation, ACI Mater. J. 88 (1991) 363–373.

[24] V.G. Papadakis, M.N. Fardis, C.G. Vayenas, Effect of composition, environmental factors and cement-lime mortar coating on concrete carbonation, Mater. Struct. 25 (1992) 293–304.

[25] E. Drouet, S. Poyet, J.-M. Torrenti, Temperature influence on water transport in hardened cement pastes, Cem. Concr. Res. 76 (2015) 37–50. doi:10.1016/j.cemconres.2015.05.002.

[26] E. Drouet, Impact de la température sur la carbonatation des matériaux cimentaires - prise en compte des transferts hydriques (in French), Ph.D. Thesis, Ecole Normale Supérieure de Cachan (France), 2010.

[27] E. Drouet, S. Poyet, P. Le Bescop, J.-M. Torrenti, X. Bourbon, Carbonation of hardened cement pastes: Influence of temperature, Cem. Concr. Res. (2019). doi:10.1016/J.CEMCONRES.2018.09.019.

[28] G.J. Verbeck, Carbonation of Hydrated Portland Cement, ASTM Spec. Tech. Publ. 205 (1958) 17–36.

[29] I. Galan, C. Andrade, M. Castellote, Natural and accelerated CO2 binding kinetics in cement paste at different relative humidities, Cem. Concr. Res. 49 (2013) 21–28. doi:10.1016/j.cemconres.2013.03.009.

[30] M. Castellote, L. Fernandez, C. Andrade, C. Alonso, Chemical changes and phase analysis of OPC pastes carbonated at different CO2 concentrations, Mater. Struct. 42 (2009) 515–525. doi:10.1617/s11527-008-9399-1.

[31] J. Sercombe, R. Vidal, C. Gallé, F. Adenot, Experimental study of gas diffusion in cement paste, Cem. Concr. Res. 37 (2007) 579–588. doi:10.1016/j.cemconres.2006.12.003.

[32] C. Boher, F. Frizon, S. Lorente, F. Bart, Influence of the pore network on hydrogen diffusion through blended cement pastes, Cem. Concr. Compos. 37 (2013) 30–36. doi:10.1016/j.cemconcomp.2012.12.009.

[33] J. Crank, The mathematics of diffusion, 2nd Ed., Clarendon Press, Oxford, 1975. doi:10.1016/0306-4549(77)90072-X.

[34] V. Baroghel-Bouny, M. Mainguy, T. Lassabatere, O. Coussy, Characterization and identification of equilibrium and transfer moisture properties for ordinary and high-performance cementitious materials, Cem. Concr. Res. 29 (1999) 1225–1238. doi:10.1016/S0008-8846(99)00102-7.

[35] L. Wadsö, K. Svennberg, A. Dueck, An experimentally simple method for measuring sorption isotherms, Dry. Technol. 22 (2004) 2427–2240.

[36] D.S. Carr, B.L. Harris, Solutions for Maintaining Constant Relative Humidity, Ind. Eng. Chem. 41 (1949) 2014–2015. doi:10.1021/ie50477a042.

[37] A. Wexler, S. Hasegawa, Relative humidity-temperature relationships of some staurated salt solutions in the temperature range 0° to 50°C, J. Res. Natl. Bur. Stand. (1934). 53 (1954) 19–26.

[38] J.F. Young, Humidity control in the laboratory using salt solutions - a review, J. Appl. Chem. 17 (1967) 241–245.

[39] L. Greenspan, Humidity fixed points of binary saturated aqueous solutions, J. Res. Natl. Bur. Stand. Sect. A Phys. Chem. 81A (1977) 89–96. doi:10.6028/jres.081A.011.

[40] R.A. Olson, H.M. Jennings, Estimation of C-S-H content in a blended cement paste using water adsorption, Cem. Concr. Res. 31 (2001) 351–356. doi:10.1016/S0008-8846(01)00454-9.

[41] G. Pickett, Modification of the Brunauer Emmett Teller Theory of Multimolecular Adsorption, J. Am. Chem. Soc. 67 (1945) 1958–1962. http://pubs.acs.org/doi/abs/10.1021/ja01227a027.

[42] G. Villain, G. Platret, Two experimental methods to determine carbonation profiles in concrete, ACI Mater. J. 103 (2006) 265–271.

[43] B. Lothenbach, P. Durdzinski, K. De Weerdt, Thermogravimetric analysis, in: L. Scrivener, Snellings (Ed.), A Pract. Guid. to Microstruct. Anal. Cem. Mater., CRC Press, Boca Raton (USA), 2016: pp. 177–211.

[44] F. Frizon, C. Gallé, Diffusive and convective transport of inert gas through cement pastes: influence of microstructure and water, J. Porous Media. 12 (2009) 221–237. doi:10.1615/JPorMedia.v12.i3.30.

[45] M. Boumaaza, B. Huet, G. Pham, P. Turcry, A. Aït-Mokhtar, C. Gehlen, A new test method to determine the gaseous oxygen diffusion coefficient of cement pastes as a function of hydration duration, microstructure, and relative humidity, Mater. Struct. 51 (2018) 51. doi:10.1617/s11527-018-1178-z.

[46] Y.F. Houst, F.H. Wittmann, Influence of porosity and water content on the diffusivity of CO2 and O2 through hydrated cement paste, Cem. Concr. Res. 24 (1994) 1165–1176. doi:10.1016/0008-8846(94)90040-X.

[47] S.W. Webb, Gas Transport Mechanisms, in: C.K. Ho, S.W. Webb (Eds.), Theory Appl. Transp. Porous Media, Springer, 2006: pp. 5–26.

[48] K. Kobayashi, K. Shuttoh, Oxygen diffusivity of various cementitious materials, Cem. Concr. Res. 21 (1991) 273–284. doi:http://dx.doi.org/10.1016/0008-8846(91)90009-7.

[49] T. Klink, K. Gaber, E. Schlattner, M.J. Setzer, Characterisation of the gas transport properties of porous materials by determining the radon diffusion coefficient, Mater. Struct. 32 (1999) 749–754.

[50] W. Ashraf, Carbonation of cement-based materials : Challenges and opportunities, Constr. Build. Mater. 120 (2016) 558–570. doi:10.1016/j.conbuildmat.2016.05.080.

[51] B. Šavija, M. Luković, Carbonation of cement paste: Understanding, challenges, and opportunities, Constr. Build. Mater. 117 (2016) 285–301. doi:10.1016/j.conbuildmat.2016.04.138.

[52] P.H.R.R. Borges, N.B. Milestone, J.O. Costa, C.J. Lynsdale, T.H. Panzera, A.L. Christophoro, Carbonation durability of blended cement pastes used for waste encapsulation, Mater. Struct. 45 (2012) 663–678. doi:10.1617/s11527-011-9788-8.

[53] A. Leemann, P. Nygaard, J. Kaufmann, R. Loser, Relation between carbonation resistance, mix design and exposure of mortar and concrete, Cem. Concr. Compos. 62 (2015) 33–43. doi:10.1016/j.cemconcomp.2015.04.020.

[54] J.L. Branch, D.S. Kosson, A.C. Garrabrants, P.J. He, The impact of carbonation on the microstructure and solubility of major constituents in microconcrete materials with varying alkalinities due to fly ash replacement of ordinary Portland cement, Cem. Concr.

Res. 89 (2016) 297–309. doi:10.1016/j.cemconres.2016.08.019.

[55] A. Leemann, F. Moro, Carbonation of concrete: the role of CO2 concentration, relative humidity and CO2 buffer capacity, Mater. Struct. 50 (2017) 30. doi:10.1617/s11527-016-0917-2.

[56] V. Shah, S. Bishnoi, Carbonation resistance of cements containing supplementary cementitious materials and its relation to various parameters of concrete, Constr. Build. Mater. 178 (2018) 219–232. doi:10.1016/j.conbuildmat.2018.05.162.

[57] K. Tuutti, Corrosion of steel in concrete, CBI Report 4.82, Swedish Cement and Concrete Research Institute, Stockholm (Sweden), 1982. doi:10.4324/9780203414606_chapter_2.

[58] D.W.S. Ho, R.K. Lewis, Carbonation of concrete and its prediction, Cem. Concr. Res. 17 (1987) 489–504.

[59] V.L. Ta, S. Bonnet, T. Senga Kiesse, A. Ventura, A new meta-model to calculate carbonation front depth within concrete structures, Constr. Build. Mater. 129 (2016) 172–181. doi:10.1016/j.conbuildmat.2016.10.103.

[60] S.O. Ekolu, Model for practical prediction of natural carbonation in reinforced concrete: Part 1-formulation, Cem. Concr. Compos. 86 (2018) 40–56. doi:10.1016/j.cemconcomp.2017.10.006.

[61] Y.F. Houst, F.H. Wittmann, Depth profiles of carbonates formed during natural carbonation, Cem. Concr. Res. 32 (2002) 1923–1930. doi:10.1016/S0008-8846(02)00908-0.

[62] C.F. Chang, J.W. Chen, The experimental investigation of concrete carbonation depth, Cem. Concr. Res. 36 (2006) 1760–1767. doi:10.1016/j.cemconres.2004.07.025.

[63] Y.S. Ji, M. Wu, B. Ding, F. Liu, F. Gao, The experimental investigation of width of semi-carbonation zone in carbonated concrete, Constr. Build. Mater. 65 (2014) 67–75. doi:10.1016/j.conbuildmat.2014.04.095.

[64] M. Thiery, G. Villain, P. Dangla, G. Platret, Investigation of the carbonation front shape on cementitious materials: Effects of the chemical kinetics, Cem. Concr. Resear. 37 (2007) 1047–1058. doi:10.1016/j.cemconres.2007.04.002.

[65] S.A. Rodger, G.W. Groves, Electron-Microscopy Study of Ordinary Portland-Cement and Ordinary Portland Cement-Pulverized Fuel Ash Blended Pastes, J. Am. Ceram. Soc. 72 (1989) 1037–1039. doi:10.1111/j.1151-2916.1989.tb06265.x.

[66] M. Atkins, E.E. Lachowski, F.P. Glasser, Investigation of solid and aqueous chemistry of 10-year-old Portland cements pastes; with and without silica modifier, Adv. Cem. Res. 5 (1993) 97–102.

[67] R. Taylor, I.G. Richardson, R.M.D. Brydson, Composition and microstructure of 20-year-old ordinary Portland cement-ground granulated blast-furnace slag blends containing 0 to 100% slag, Cem. Concr. Res. 40 (2010) 971–983. doi:10.1016/j.cemconres.2010.02.012.

[68] Q. Wang, J. Feng, P. Yan, The microstructure of 4-year-old hardened cement-fly ash paste, Constr. Build. Mater. 29 (2012) 114–119. doi:10.1016/j.conbuildmat.2011.08.088.

[69] M. Codina, C. Cau-dit-Coumes, P. Le Bescop, J. Verdier, J.P. Ollivier, Design and characterization of low-heat and low-alkalinity cements, Cem. Concr. Res. 38 (2008) 437–448. doi:10.1016/j.cemconres.2007.12.002.

[70] A. Dauzères, P. Le Bescop, C. Cau-Dit-Coumes, F. Brunet, X. Bourbon, J. Timonen, M. Voutilainen, L. Chomat, P. Sardini, On the physico-chemical evolution of low-pH and CEM I cement pastes interacting with Callovo-Oxfordian pore water under its in situ CO2 partial pressure, Cem. Concr. Res. 58 (2014) 76–88. doi:10.1016/j.cemconres.2014.01.010.

[71] V.G. Papadakis, M.N. Fardis, C.G. Vayenas, Hydration and carbonation of pozzolanic cements, ACI Mater. J. 89 (1992) 119–130.

[72] V.G. Papadakis, Effect of supplementary cementing materials on concrete resistance against carbonation and chloride ingress, Cem. Concr. Res. 30 (2000) 291–299.

[73] C.-Q. Lye, R.K. Dhir, G.S. Ghataora, Carbonation resistance of GGBS concrete, Mag. Concr. Res. 68 (2016) 936–969. doi:10.1680/jmacr.15.00449.

[74] C.-Q. Lye, G.S. Ghataora, R.K. Dhir, Carbonation resistance of fly ash concrete, Mag. Concr. Res. 67 (2015) 1150–1178.